Since January 2020 Elsevier has created a COVID-19 resource centre with free information in English and Mandarin on the novel coronavirus COVID-19. The COVID-19 resource centre is hosted on Elsevier Connect, the company's public news and information website.

Journal of Colloid and Interface Science 600 (2021) 613–619

Contents lists available at ScienceDirect

Journal of Colloid and Interface Science

journal homepage: www.elsevier.com/locate/jcis

Regular Article

Superhydrophobicity preventing surface contamination as a novel strategy against COVID-19

Pingan Zhu [a,b,c,1], Yixin Wang [d,1], Hin Chu [d,*], Liqiu Wang [b,c,*]

[a] Department of Mechanical Engineering, City University of Hong Kong, Hong Kong, China
[b] Department of Mechanical Engineering, the University of Hong Kong, Hong Kong, China
[c] HKU-Zhejiang Institute of Research and Innovation (HKU-ZIRI), 311300 Hangzhou, China
[d] Department of Microbiology, Li Ka Shing Faculty of Medicine, the University of Hong Kong, Hong Kong, China

GRAPHICAL ABSTRACT

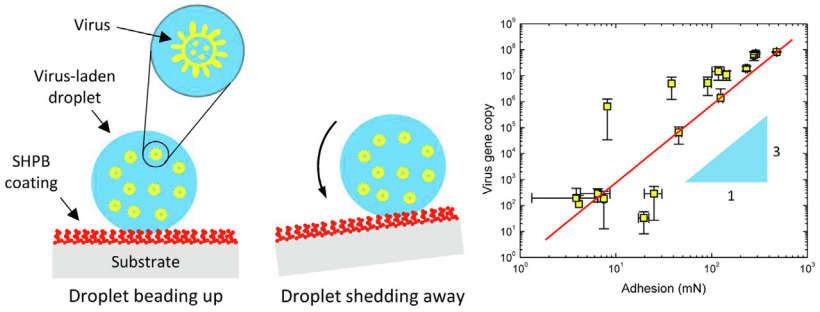

ARTICLE INFO

Article history:
Received 12 January 2021
Revised 12 April 2021
Accepted 6 May 2021
Available online 11 May 2021

Keywords:
COVID-19
SARS-CoV-2
Superhydrophobicity
Surface contamination
Fomite transmission

ABSTRACT

Surface contact with virus is ubiquitous in the transmission pathways of respiratory diseases such as Coronavirus Disease 2019 (COVID-19), by which contaminated surfaces are infectious fomites intensifying the transmission of the disease. To date, the influence of surface wettability on fomite formation remains elusive. Here, we report that superhydrophobicity prevents the attachment of severe acute respiratory syndrome coronavirus 2 (SARS-CoV-2) on surfaces by repelling virus-laden droplets. Compared to bare surfaces, superhydrophobic (SHPB) surfaces exhibit a significant reduction in SARS-CoV-2 attachment of up to 99.99995%. We identify the vital importance of solid-liquid adhesion in dominating viral attachment, where the viral activity (N) is proportional to the cube of solid-liquid adhesion (A), $N \propto A^3$. Our results predict that a surface would be practically free of SARS-CoV-2 deposition when solid-liquid adhesion is $\leq$1 mN. Engineering surfaces with superhydrophobicity would open an avenue for developing a general approach to preventing fomite formation against the COVID-19 pandemic and future ones.

1. Introduction

Infectious diseases are caused by pathogenic microbes (such as bacteria, viruses, parasites or fungi) that invade the human body to reproduce or release toxins, which damage host cells and their functions and even lead to death in severe cases. Human society has been plagued by infectious diseases; well-known epidemics,

* Corresponding authors at: Department of Mechanical Engineering, the University of Hong Kong, Hong Kong, China (L. Wang); Department of Microbiology, Li Ka Shing Faculty of Medicine, the University of Hong Kong, Hong Kong, China (H. Chu).
E-mail addresses: hinchu@hku.hk (H. Chu), lqwang@hku.hk (L. Wang).
[1] These authors contributed equally to this work.

https://doi.org/10.1016/j.jcis.2021.05.031
0021-9797/

such as the Black Death, smallpox, yellow fever and cholera, have irreversibly shaped the course of human history and caused incalculable deaths [1]. New epidemics continue to emerge. Since the emergence of Coronavirus Disease 2019 (COVID-19), which is caused by severe acute respiratory syndrome coronavirus 2 (SARS-CoV-2), the disease has rapidly evolved into a global pandemic in several months [2,3]. As this paper is being prepared, COVID-19 continues to prevail globally, resulting in more than 160 million confirmed cases and over 3.3 million deaths in more than 210 countries and regions. Before safe and effective vaccines are available [4], COVID-19 is likely to remain with humans for a long time and will have a profound impact on public health, global economy, and the way of life [5]. Mitigation measures to prevent the transmission of COVID-19 are of vital importance to fighting the pandemic.

Respiratory diseases (such as COVID-19) can be transmitted through either airborne or contact routes [6,7]. As a start, virus-laden respiratory droplets (from <1 to 2000 μm in diameter [6]) are released from infectious individuals when they are coughing, sneezing, talking, singing and even exhaling. Then the virus-laden airborne droplets are inhaled by other individuals for direct infection or deposited on persons/objects to turn surfaces into infectious fomites, which may cause indirect infection when someone touches the contaminated surfaces by hands and then transfers the virus to eyes, nose, and mouth. Virus-surface contact plays an important role in fomite transmission [8]. SARS-CoV-2 exhibits a strong capability of surviving in the environment, remaining infectious for 4–7 days on surfaces like glass, plastics, stainless steel, and the outer layer of a surgical mask [6,9,10]. Thus, it is urgently needed to develop functional surfaces for preventing fomite transmission.

Suppressing fomite formation could effectively interrupt the fomite-to-human transmission. Given that fomites involve the deposition of virus-laden aqueous droplets on surfaces, it is envisaged that superhydrophobic (SHPB) surfaces hold great promise for setting physical barriers that avoid the adhering of virus-laden droplets [11]. SHPB surfaces are featured by high water contact angle (CA > 150°) and low contact angle hysteresis (CAH < 10°) [12]. Water droplets are supported by micro- or nano-structures on SHPB surfaces, maintained in the non-wetted Cassie state [13]. As such, a large fraction of solid-liquid contact is replaced by liquid-air interfaces on SHPB surfaces. Due to the reduced solid-liquid interactions, SHPB surfaces allow a strong mobility of water droplets useful for various applications, such as self-cleaning, anti-biofouling, and droplet manipulation [14–20]. Such functional surfaces have been demonstrated to have antimicrobial characteristics [21–23], on which bacteria is prevented from adhesion/attachment. It is thus expected that engineering surfaces with superhydrophobicity could be developed into a general approach to preventing viral adhesion, not limited to a specific type of pathogens. However, the efficacy of superhydrophobicity against fomite infection remains elusive and unavailable.

Here, we investigate the influence of superhydrophobicity on fomite formation of COVID-19. In a systematic study, we conduct viral adhesion tests on six commonly-used substrates (copper, glass, glove, face mask, plastic, and steel) with different wettability. The viral adhesion is not determined by the static CAs, but instead by the dynamic CAs that characterize the solid-liquid adhesion. According to experimental results, the amount of attached virus is proportional to the cube of solid-liquid adhesion. The quantitative relationship also predicts that no virus will practically remain on SHPB surfaces when the adhesion is reduced to $\leq$1 mN. As such, SHPB surfaces with lower adhesion exhibit a significant reduction in viral adhesion. Our work would provide useful guidelines in engineering surface wettability for interrupting fomite-to-human transmission in fighting COVID-19 and other epidemics.

2. Materials and methods

2.1. Fabrication of SHPB coatings

The Glaco coating (SOFT99, GLACO) solution was used as received. The Aerosil coating solution was prepared by dispersing hydrophobic silica nanoparticles (AEROSIL® fumed silica) in ethanol at a concentration of 2.5 w/w%. Both coatings are composed of silanized silica nanoparticles that have similar size distribution (diameter ranging from ~20 to ~40 nm) and comparable average diameter (~30 nm). The two coatings were applied to the substrates by dip coating and each substrate was dip-coated three times to ensure that all the surface areas were covered by nanoparticle assemblies. After coating, the substrate was rendered SHPB.

2.2. Viruses and biosafety

SARS-CoV-2 HKU-001a was isolated from a COVID-19 patient from Hong Kong as we previously described [24]. The virus was expanded in VeroE6 cells in Dulbecco's Modified Eagle Medium (DMEM). On the day of virus harvest, the culture supernatant was centrifuged at 2000 rounds per minute (rpm) to remove cell debris, and the virus titer was determined by plaque assays as we previously described [25]. All experiment protocol follows the standard operating procedures of Biosafety Level 3 facility at the Department of Microbiology, University of Hong Kong [26]. Inactivated SARS-CoV-2 was prepared by incubating SARS-CoV-2 with 4% paraformaldehyde. The lack of infectious virus titer of inactivated SARS-CoV-2 was determined with median tissue culture infectious dose ($TCID_{50}$) assays on VeroE6 cells.

2.3. Viral adhesion test

50 μL of infectious SARS-CoV-2 in DMEM at a concentration of 1×10^7 PFU/mL was applied to each surface. At 5 min after adding the virus, the surfaces were tilted to allow free falling of the virus droplet. The surfaces were then added to phosphate-buffered saline (PBS) and were incubated for 30 min before the PBS was harvested and lyzed for viral RNA extraction.

2.4. RNA extraction and qRT-PCR

RNA extraction and qRT-PCR were performed as we previously described [27]. In brief, residual SARS-CoV-2 on different surfaces was extracted with the QIAamp Viral RNA Mini kits (Qiagen, Hilden, Germany). Quantitative RT-PCR was performed using the QuantiNova Probe RT-PCR kit (Qiagen) with LightCycler 480 Real-Time PCR System (Roche, Basel, Switzerland). The primer and probe sequences were previously described [28,29].

2.5. Characterization of surface wettability

The static CAs, dynamic CAs and sliding angles were measured by the OCA 25 instrument (DataPhysics) at room temperature (23 °C). The static and dynamic CAs were the average of 5 measurements at different positions on the surface. The sliding angles were the average of 3 replicates.

A 5 μL droplet was firstly deposited on the surface, then a side-view image was taken, and finally the static CA was analyzed by the software of OCA.

To measure the dynamic CA, a droplet of 5 μL was firstly deposited on the surface. Then, another 10 μL liquid was slowly pumped in and out of the droplet at a rate of 1 μL/s, during which the contact line advances and recedes, respectively. A video was recorded for the process and the advancing CA and receding CA were ana-

lyzed by the software of OCA. CAH is defined and calculated as the difference between advancing CA and receding CA.

To measure the sliding angle, the surface was placed on a tilting stage. A 10 μL droplet was deposited on the surface. Then the stage was tilted slowly to let the droplet roll off. A video was recorded. When the droplet started to slide, the surface tilting angle indicated the sliding angle.

The solid–liquid adhesion was measured by the DCAT device (DataPhysics Instruments). A 10 μL droplet was used to firstly snap in and then snap off the tested surface. During snapping in, the droplet was compressed by 0.5 mm at a constant speed of 0.05 mm/s, after which the droplet was snapped off at the same speed. The software automatically recorded the force curve and calculated the maximum force for the solid-liquid adhesion.

2.6. Quantification of liquid residue ratio

The liquid residue ratio was measured by DCAT 25 instrument (DataPhysics) with the same process as the measurement of solid-liquid adhesion. From the recorded force curve, we extracted the initial force before snapping in and the final force after snapping off. The difference between the two forces equals the weight of liquid residue left on the tested surface. The mass of liquid residue m_r was then calculated by dividing the force difference by the gravitational acceleration g. The measurement accuracy can reach 10^{-5} g. The initial mass of the droplet m_0 was kept as a constant by controlling the droplet volume to be 10 μL.

2.7. Mechanical stability test

We used a sandpaper abrasion test to characterize the durability of SHPB coatings. The coated substrate was placed on top of a sandpaper and had the SHPB coating side facing the sandpaper. A weight was placed on the substrate to exert an applied pressure of 1.7 kPa. For each cycle of the abrasion test, the substrate (with the loaded weight) was forced to move on the sandpaper for a distance of 5 cm. After abrasion, the static CA was measured.

3. Results and discussion

Fig. 1a illustrates the principle of preventing fomite formation using SHPB coatings. A virus-laden droplet will bead up on the coating in the non-wetted Cassie state [13], by which numerous air pockets are sandwiched between the droplet and the SHPB coating, significantly reducing the area of solid-liquid contact and the virus-surface contact probability. In the SHPB state, the virus-laden droplet readily rolls off the tilted surface such that virus can barely remain on the coating. Covered with SHPB coatings, the underneath substrates are then protected from the deposition of virions, which greatly eliminates the production of fomites to effectively prevent the transmission of virus.

We prepared two SHPB coatings using two types of silanized silica nanoparticles, which are referred to as Glaco coating and Aerosil coating and shown in Fig. 1b (SOFT99, GLACO) and 1c (AEROSIL® fumed silica), respectively. Compared to the Glaco coating (Fig. 1b), nanoparticle assemblies are fluffier on the Aerosil coating (Fig. 1c). The presence of the two coatings significantly alters the wettability of the surface. Fig. 1d contrasts the CAs of aqueous droplets containing inactivated SARS-CoV-2, where the droplet wets the bare glass substrate (CA < 30°) while beads up on both Glaco and Aerosil coated glasses (CA > 150°). Moreover, SHPB coatings demonstrate the repellency to aqueous droplets with an average radius of ~35 μm (Fig. S1 and Movie S1), suggesting the possibility of shedding tiny virus-laden respiratory droplets.

To examine the efficacy of SHPB coatings against SARS-CoV-2 for the protection of diverse objects and systematically study the influence of surface wettability, we investigated six commonly-used materials and PPE—copper, glass, glove, face mask (the outer layer), plastic, and steel—in three groups: bare substrate, Glaco coating, and Aerosil coating. The SHPB coatings are uniform on smooth surfaces including copper, glass, glove, plastic, and steel (Fig. S2), but less uniform on face mask (Fig. S3). Fig. 1e shows the images of water (blue) and inactivated virus-laden (transparent) droplets on the 18 tested surfaces, where all droplets bead up on SHPB surfaces whereas the droplets wet all bare substrates except face mask (because the outer layer of face mask is hydrophobic). As contrasted in Fig. 1f, the values of CAH are the largest on bare substrates, the smallest on Aerosil coatings, and moderate on Glaco coatings.

Fig. 2 shows the survival behavior of SARS-CoV-2 on 18 tested surfaces. Compared to SHPB coatings, all bare substrates exhibit the highest viral activity, with a log number in the range of 7–8 (Fig. 2a). Interestingly, more virus residues are left on Glaco coatings than Aerosil coatings; the log number is in the range of 5–7 on the former coatings while in the range of 2–3 on the latter coatings (Fig. 2a). In comparison to bare substrates, the viral activity is significantly reduced on SHPB coatings; the reduction is 99.997–99.99995% on Aerosil coatings while 23.6–99.4% on Glaco coatings (Fig. 2b). More remarkably, there appear several zero readings of virial activity on Aerosil coatings (Table S1, Supporting Information), suggesting the complete prevention of virus attachment. These results confirm that SHPB coatings can inhibit the formation of fomites. Nevertheless, the significant difference (approximately four orders of magnitude) between Glaco coatings and Aerosil coatings in viral activity seems counterintuitive because both coatings have similar CAs (Fig. 1d and Fig. S4) and thus raises a question about the mechanism underlying the prevention of viral adhesion.

To understand the role of superhydrophobicity in inhibiting fomite formation, we systematically studied the wettability of all tested surfaces, including static CAs, dynamic CAs (advancing CAs and receding CAs), adhesion forces, and sliding angles, as shown in Fig. 3. Fig. 3a contrasts the static CAs, where Glaco coatings have slightly larger CAs than Aerosil coatings in most cases, and both have CAs larger than bare substrates. Fig. 3b shows the dynamic CAs, in which the CAH decreases in the order of "bare substrates > Glaco coatings > Aerosil coatings" in most cases (Fig. 1f), a descending order that is highly consistent with the viral activity results. In parallel, the solid-liquid adhesion (Fig. 3c) and sliding angle (Fig. 3d) follow the same descending order. The different adhesion of Glaco and Aerosil coatings is ascribed to the morphology of nanoparticle assemblies. Different from Glaco coatings with single-tier nano-structures, Aerosil coatings have hierarchical micro-/nano-structures consisting of microscale papillae and fused silica nanoparticles with branched, chainlike, and three-dimensional morphology (Fig. 1b, 1c, and S2). As such, Aerosil coatings are rougher and thus achieve lower adhesion and better water repellency than Glaco coatings.

Given that CAH, adhesion, and sliding angle are parameters characterizing how sticky a surface is, we speculate that viral adhesion is dominated by the sticky state of the surface rather than by the static CA. A less sticky surface is expected to perform better in preventing viral adhesion. To verify our hypothesis, we plotted the viral activity results versus the static CA and adhesion in Fig. 3e and 3f, respectively. The data in Fig. 3e is separated into two distinct groups: the viral activity has a log number in the range of 7–8 for all CAs < 100° and in a wide range of 1–7 when CA = 150° or so. Such differentiation of data indicates that there is no significant correlation between viral activity and static CA.

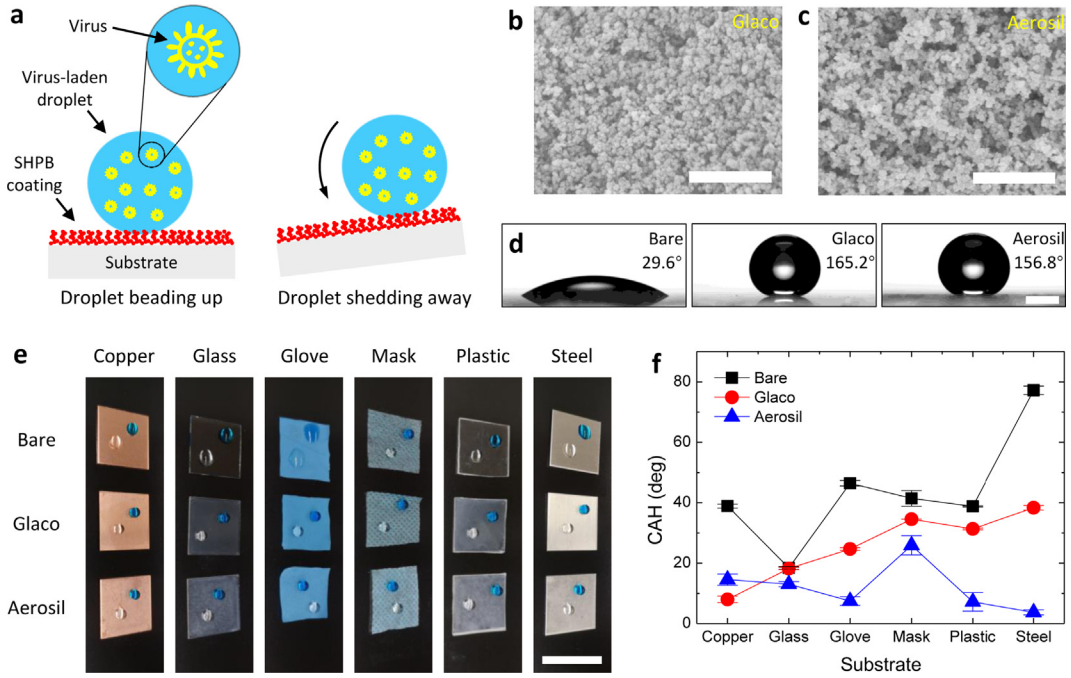

Fig. 1. Prevention of fomite formation by superhydrophobicity. (a) Schematic (not to scale) showing that the virus-laden droplet beads up on the leveled SHPB coating and rolls off the tilted SHPB coating which avoids virus deposition for preventing fomite formation. (b-c) Scanning electron microscope (SEM) images for the Glaco (b) and Aerosil (c) coatings. (d) Optical images showing contact angles (CAs) of inactivated virus-laden droplets on bare glass substrate, Glaco coating, and Aerosil coating. The glass substrate is changed from hydrophilic to SHPB. (e) Pictures contrasting the contact of water (blue) and inactivated virus-laden (transparent) droplets on 18 tested surfaces. (f) Contact angle hysteresis (CAH) on different substrates. Scale bars, 500 nm in (b-c), 1 mm in (d), and 2 cm in (e). (For interpretation of the references to colour in this figure legend, the reader is referred to the web version of this article.)

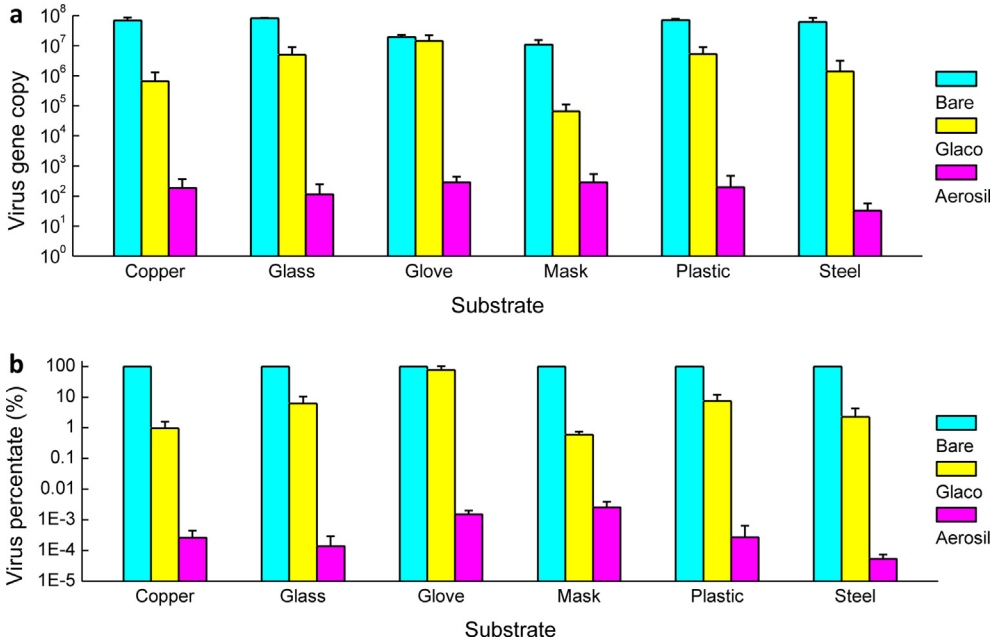

Fig. 2. Viral activity test of SARS-CoV-2. (a) Virus gene copy versus different surfaces. Viral activity decreases in the order of "bare substrates > Glaco coatings > Aerosil coatings" for each substrate. The virus gene copy is the average of three replicates. (b) Relative viral activity versus different surfaces. For each substrate, the viral activity is normalized by the virus gene copy of bare substrate. As such, the virus percentage is always 100% and the error bar is 0 for bare substrate.

In contrast, viral activity is positively correlated with adhesion, as shown in Fig. 3f. More remarkably, the curve fitting unveils that viral activity (N) is proportional to the cube of adhesion (A), $N \propto A^3$. This quantitative relationship emphasizes the vital importance of adhesion in preventing fomite formation: a 10-time variation in the adhesion will dramatically lead to a 1000-time change in the viral activity. Compared to bare substrates, Aerosil coatings have the adhesion decreased by ~2 orders of magnitude to ~10 mN, so that the viral activity is reduced by 5–6 orders of magnitude, which explains the observed significant reduction in Fig. 2. The Aerosil coating is less sticky than the Glaco coating (Fig. 3c, 3d, and S5), so that the former demonstrates a better ability to prevent fomite

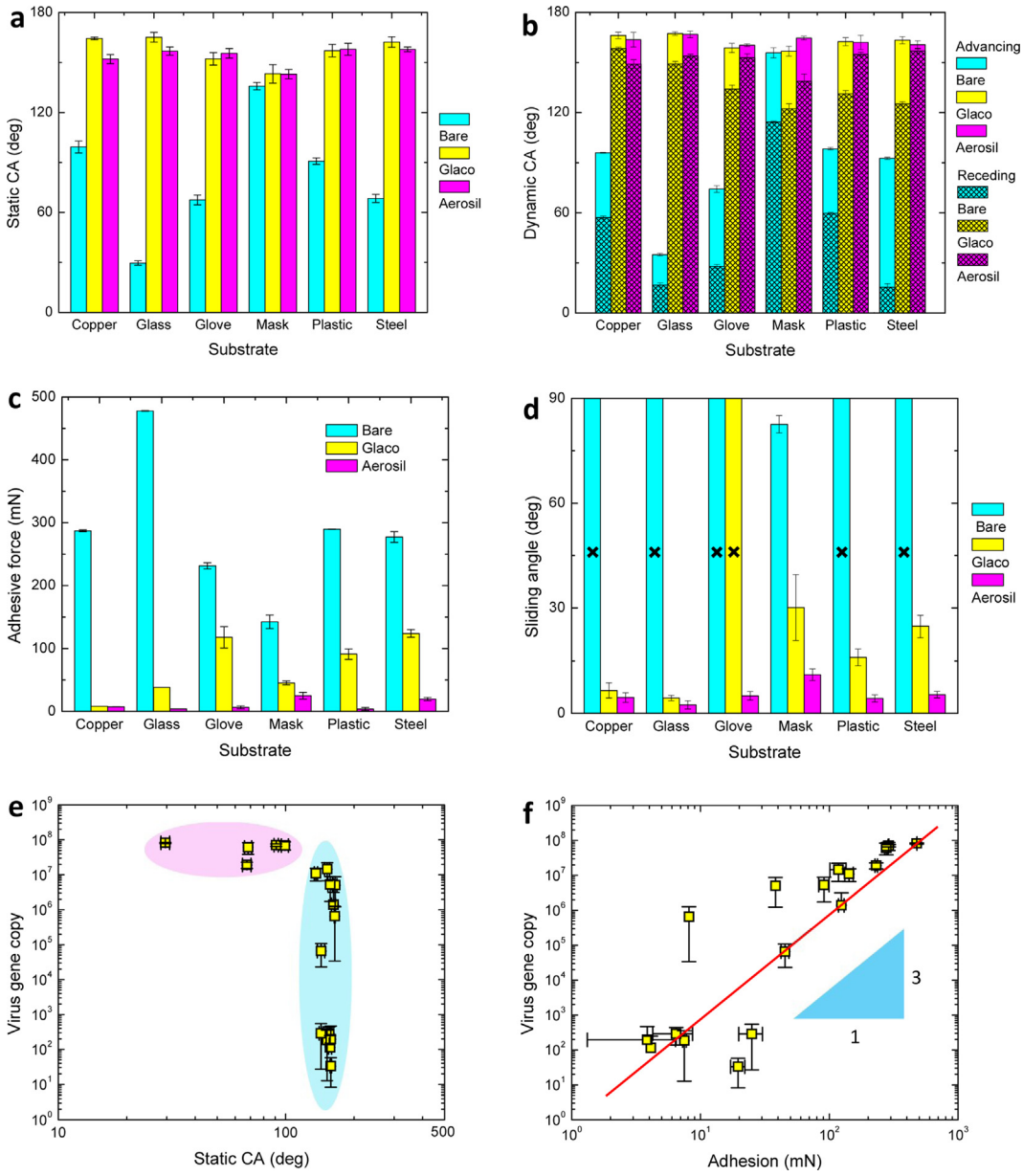

Fig. 3. Correlation between surface wettability and viral adhesion. (a-d) Static CA (a), dynamic CA (b), solid-liquid adhesion (c), and sliding angle (d) for different surfaces. The droplet cannot slide the 90°-tilted surface in some cases due to the very large adhesion, which is marked with a "×" in (d). (e) The plot of virus gene copy versus the static CA. The data is separated into two different groups, as encompassed in the two ellipses. (f) The plot of virus gene copy versus adhesion. The curve fitting (solid line) indicates that viral activity is proportional to the cube of adhesion.

formation than the latter. More importantly, the curve fitting predicts that there would be no virus left on SHPB coatings when the adhesion is decreased to $\leq$1 mN in the present test, because the initial ~10^8 residual virus gene copy on bare substrates will be reduced by 9 orders of magnitude to ~0.1, much smaller than unity. Indeed, Aerosil coatings with the adhesion of ~10 mN occasionally exhibit complete prevention of virus attachment in experiments (Table S1).

For a less sticky surface with lower adhesion, there would be fewer residues of virus-laden liquid left after contact, which is thus endowed with better performance in preventing viral adhesion. We characterized the liquid residue on different surfaces in Fig. 4. Virus residue is observed on both bare substrate (Fig. 4a) and Glaco coating (Fig. 4b) while almost no residue can be found on Aerosil coating (Fig. 4c) after the surface is deposited with a virus-laden droplet and then tilted. We quantified the mass ratio (m_r/m_0) of liquid residue (mass m_r) by controlling a liquid droplet (mass m_0) firstly snapping in and then snapping off the surface (Fig. 4d). The results are shown in Fig. 4e, where bare substrates have the residue ratio m_r/m_0 > 70% except for face mask (because the outer layer of face mask is hydrophobic), while Aerosil coatings have m_r/m_0 < 1% and Glaco coatings have m_r/m_0 with a value in between. The liquid residue characterization is consistent with the sticky and viral activity test, all of which together confirm that surfaces with lower adhesion would be better in preventing fomite formation.

The durability of superhydrophobicity is one of the important factors to be considered because long-term ability to prevent fomite formation is desired in practice. We performed a sandpaper abrasion test to examine the mechanical stability of SHPB coatings, which can withstand 20 cycles of abrasion under an applied load of 1.7 kPa (Fig. S6). Besides, superhydrophobicity is retained on

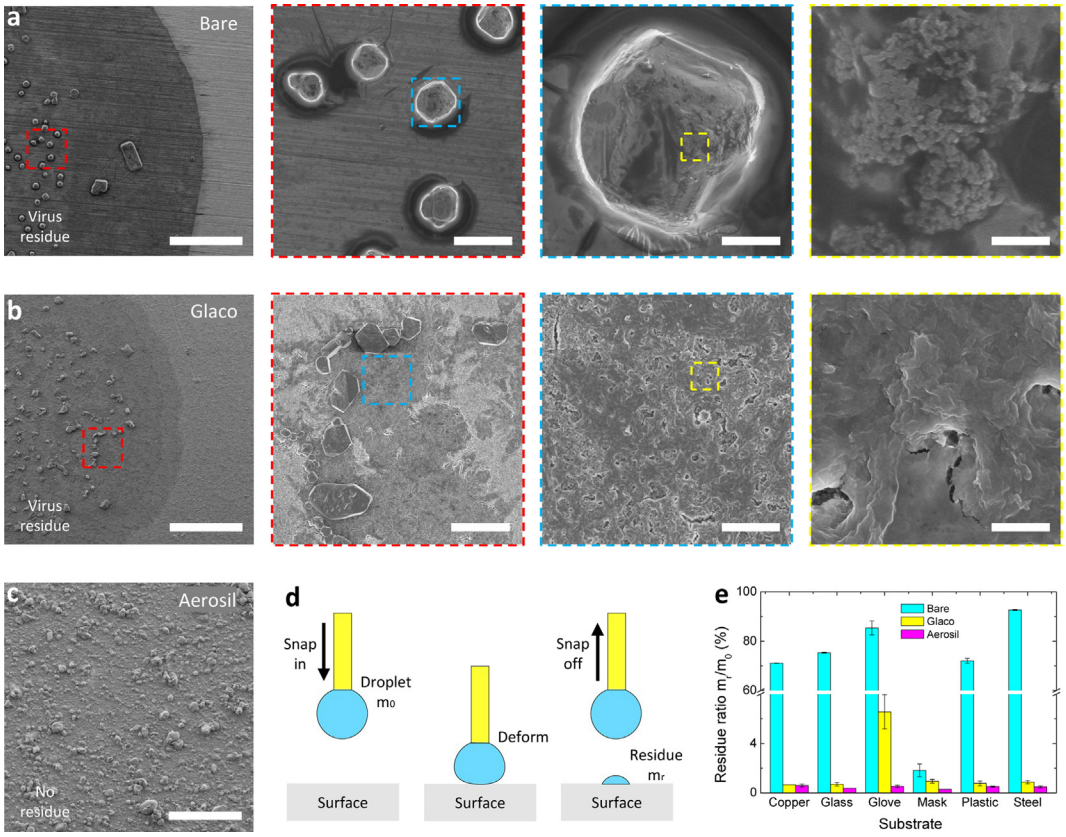

Fig. 4. Liquid residues on surfaces with different wettability. (a-b) SEM images showing virus residues on the bare substrate (a) and Glaco coating (b). The boundaries separating the virus residue and the pristine surface are observed in the leftmost images of (a-b). The granular and membranous residues come from the additives in the virus-laden liquid. (c) No observation of virus liquid residue on Aerosil coating owing to the low adhesion. (d) Schematic showing the measurement of residue ratio m_r/m_0, where m_r and m_0 are the mass of liquid residue and droplet, respectively. (e) The plot of residue ratio m_r/m_0 versus different surfaces. The residue is the average of three replicates. Scale bars, 500 μm, 50 μm, 10 μm and 1 μm for images from left to right in (a-b) and 500 μm in (c).

deformed surfaces, as demonstrated by the bouncing of aqueous droplets on curved glove and face mask (Fig. S7 and Movie S2). To further improve the durability, one can adopt useful strategies available in the literature: recent studies have proposed robust liquid-repellent surfaces by either optimizing the topological design [30,31] or using all-organic nanocomposite coating [32].

4. Conclusions

We have confirmed the effectiveness of superhydrophobicity in preventing fomite formation by repelling virus-laden droplets. The viral attachment is dominated by and proportional to the cube of solid-liquid adhesion. As such, a surface with lower adhesion offers better prevention of viral contamination. Remarkably, our results predict that a surface would be free of SARS-CoV-2 deposition when the adhesion is $\leq$1 mN, in which case the fomite formation is completely suppressed for effectively preventing the fomite-to-human transmission of COVID-19. Engineering surfaces with superhydrophobicity represents an innovative and general approach that circumvents issues encountered by other protection and disinfection measures. For example, the massive use of personal protective equipment (PPE) will lead to an increase in non-biodegradable plastics waste [6,8,33]; chemical sanitization using disinfectants needs intensive labor, consumes many materials, requires periodical repetition, can cause skin, eye and respiratory diseases, pollute the environment, and is difficult to cover all areas [6,11]. Further efforts can be devoted to imparting superhydrophobicity to various substrates and materials for practical usages, such as developing SHPB reusable PPE.

CRediT authorship contribution statement

Pingan Zhu: Conceptualization, Methodology, Investigation, Visualization, Writing - original draft, Writing - review & editing. **Yixin Wang:** Investigation, Visualization. **Hin Chu:** Conceptualization, Methodology, Resources, Writing - original draft. **Liqiu Wang:** Conceptualization, Methodology, Resources, Writing - original draft, Writing - review & editing, Supervision, Funding acquisition.

Declaration of competing interest

The authors declare that they have no known competing financial interests or personal relationships that could have appeared to influence the work reported in this paper.

Acknowledgements

The financial support from the Research Grants Council of Hong Kong (GRF 17204420, 17123920, 17210319, 17204718, 17237316, CRF C1006-20WF and C1018-17G, and TRS T11/707/15) and City University of Hong Kong (9610502) is gratefully acknowledged. This work was also supported in part by the Zhejiang Provincial, Hangzhou Municipal, and Lin'an County Governments.

Appendix A. Supplementary data

Supplementary data to this article can be found online at https://doi.org/10.1016/j.jcis.2021.05.031.

References

[1] D.M. Morens, G.K. Folkers, A.S. Fauci, The challenge of emerging and re-emerging infectious diseases, Nature 430 (2004) 242–249.

[2] J.F.-W. Chan, S. Yuan, K.-H. Kok, K.K.-W. To, H. Chu, J. Yang, F. Xing, J. Liu, C.C.-Y. Yip, R.W.-S. Poon, H.-W. Tsoi, S.K.-F. Lo, K.-H. Chan, V.K.-M. Poon, W.-M. Chan, J.D. Ip, J.-P. Cai, V.C.-C. Cheng, H. Chen, C.K.-M. Hui, K.-Y. Yuen, A familial cluster of pneumonia associated with the 2019 novel coronavirus indicating person-to-person transmission: A study of a family cluster, Lancet 395 (2020) 514-523.

[3] N. Zhu, D. Zhang, W. Wang, X. Li, B. Yang, J. Song, X. Zhao, B. Huang, W. Shi, R. Lu, P. Niu, F. Zhan, X. Ma, D. Wang, W. Xu, G. Wu, G.F. Gao, W. Tan, A novel coronavirus from patients with pneumonia in China, 2019, New Engl. J. Med. 382 (2020) 727-733.

[4] L. Corey, J.R. Mascola, A.S. Fauci, F.S. Collins, A strategic approach to COVID-19 vaccine R&D, Science 368 (2020) 948–950.

[5] A.P. Dobson, S.L. Pimm, L. Hannah, L. Kaufman, J.A. Ahumada, A.W. Ando, A. Bernstein, J. Busch, P. Daszak, J. Engelmann, M.F. Kinnaird, B.V. Li, T. Loch-Temzelides, T. Lovejoy, K. Nowak, P.R. Roehrdanz, M.M. Vale, Ecology and economics for pandemic prevention, Science 369 (2020) 379–381.

[6] H. Huang, C. Fan, M. Li, H.L. Nie, F.B. Wang, H. Wang, R. Wang, J. Xia, X. Zheng, X. Zuo, J. Huang, COVID-19: A call for physical scientists and engineers, ACS Nano 14 (2020) 3747–3754.

[7] R. Zhang, Y. Li, A.L. Zhang, Y. Wang, M.J. Molina, Identifying airborne transmission as the dominant route for the spread of COVID-19, Proc. Natl. Acad. Sci. U.S.A. 117 (2020) 14857–14863.

[8] W.C.K. Poon, A.T. Brown, S.O.L. Direito, D.J.M. Hodgson, L. Le Nagard, A. Lips, C. E. MacPhee, D. Marenduzzo, J.R. Royer, A.F. Silva, J.H.J. Thijssen, S. Titmuss, Soft matter science and the COVID-19 pandemic, Soft Matter 16 (2020) 8310–8324.

[9] N. van Doremalen, T. Bushmaker, D.H. Morris, M.G. Holbrook, A. Gamble, B.N. Williamson, A. Tamin, J.L. Harcourt, N.J. Thornburg, S.I. Gerber, Aerosol and surface stability of SARS-CoV-2 as compared with SARS-CoV-1, New Engl. J. Med. 382 (2020) 1564–1567.

[10] A.W.H. Chin, J.T.S. Chu, M.R.A. Perera, K.P.Y. Hui, H.-L. Yen, M.C.W. Chan, M. Peiris, L.L.M. Poon, Stability of SARS-CoV-2 in different environmental conditions, Lancet Microbe 1 (2020) e10.

[11] Z. Sun, K. Ostrikov, Future antiviral surfaces: Lessons from COVID-19 pandemic, Sustain. Mater. Technol. 25 (2020) e00203.

[12] M. Liu, S. Wang, L. Jiang, Nature-inspired superwettability systems, Nat. Rev. Mater. 2 (2017) 17036.

[13] A.B.D. Cassie, S. Baxter, Wettability of porous surfaces, Trans. Faraday Soc. 40 (1944) 546–551.

[14] W. Barthlott, C. Neinhuis, Purity of the sacred lotus, or escape from contamination in biological surfaces, Planta 202 (1997) 1–8.

[15] L. Jiang, Y. Zhao, J. Zhai, A lotus-leaf-like superhydrophobic surface: a porous microsphere/nanofiber composite film prepared by electrohydrodynamics, Angew. Chem. 116 (2004) 4438–4441.

[16] P.A. Zhu, R.F. Chen, L.Q. Wang, Topography-directed hot-water super-repellent surfaces, Adv. Sci. 6 (2019) 1900798.

[17] J. Wang, L. Sun, M. Zou, W. Gao, C. Liu, L. Shang, Z. Gu, Y. Zhao, Bioinspired shape-memory graphene film with tunable wettability, Sci. Adv. 3 (2017) e1700004.

[18] X. Zhang, L. Sun, Y. Wang, F. Bian, Y. Wang, Y. Zhao, Multibioinspired slippery surfaces with wettable bump arrays for droplets pumping, Proc. Natl. Acad. Sci. U.S.A. 116 (2019) 20863–20868.

[19] L. Sun, F. Bian, Y. Wang, Y. Wang, X. Zhang, Y. Zhao, Bioinspired programmable wettability arrays for droplets manipulation, Proc. Natl. Acad. Sci. U.S.A. 117 (2020) 4527–4532.

[20] P.A. Zhu, C.M. Chen, K. Nandakumar, L.Q. Wang, Nonspecular reflection of droplets, Small 17 (2021) 2006695.

[21] L. Děkanovský, R. Elashnikov, M. Kubiková, B. Vokatá, V. Švorčík, O. Lyutakov, Dual-action flexible antimicrobial material: switchable self-cleaning, antifouling, and smart drug release, Adv. Funct. Mater. 29 (2019) 1901880.

[22] R. Jiang, L. Hao, L. Song, L. Tian, Y. Fan, J. Zhao, C. Liu, W. Ming, L. Ren, Lotus-leaf-inspired hierarchical structured surface with non-fouling and mechanical bactericidal performances, Chem. Eng. J. 398 (2020) 125609.

[23] J.K. Oh, X. Lu, Y. Min, L. Cisneros-Zevallos, M. Akbulut, Bacterially antiadhesive, optically transparent surfaces inspired from rice leaves, ACS Appl. Mater. Interfaces 7 (2015) 19274–19281.

[24] H. Chu, J.F.-W. Chan, T.T.-T. Yuen, H. Shuai, S. Yuan, Y. Wang, B. Hu, C.C.-Y. Yip, J.O.-L. Tsang, X. Huang, Y. Chai, D. Yang, Y. Hou, K.K.-H. Chik, X. Zhang, A.Y.-F. Fung, H.-W. Tsoi, J.-P. Cai, W.-M. Chan, J.D. Ip, A.W.-H. Chu, J. Zhou, D.C. Lung, K.-H. Kok, K.K.-W. To, O.T.-Y. Tsang, K.-H. Chan, K.-Y. Yuen, Comparative tropism, replication kinetics, and cell damage profiling of SARS-CoV-2 and SARS-CoV with implications for clinical manifestations, transmissibility, and laboratory studies of COVID-19: An observational study, Lancet Microbe 1 (2020) e14–e23.

[25] H. Chu, J.F.-W. Chan, Y. Wang, T.T.-T. Yuen, Y. Chai, Y. Hou, H. Shuai, D. Yang, B. Hu, X. Huang, X. Zhang, J.-P. Cai, J. Zhou, S. Yuan, K.-H. Kok, K.K.-W. To, I.H.-Y. Chan, A.J. Zhang, K.-Y. Sit, W.-K. Au, K.-Y. Yuen, Comparative replication and immune activation profiles of SARS-CoV-2 and SARS-CoV in Human Lungs: An ex vivo study with implications for the pathogenesis of COVID-19, Clin. Infect. Dis. 71 (2020) 1400–1409.

[26] H. Chu, B. Hu, X. Huang, Y. Chai, D. Zhou, Y. Wang, H. Shuai, D. Yang, Y. Hou, X. Zhang, T.T.-T. Yuen, J.-P. Cai, A.J. Zhang, J. Zhou, S. Yuan, K.K.-W. To, I.H.-Y. Chan, K.-Y. Sit, D.C.-C. Foo, I.Y.-H. Wong, A.T.-L. Ng, T.T. Cheung, S.Y.-K. Law, W.-K. Au, M.A. Brindley, Z. Chen, K.-H. Kok, J.F.-W. Chan, K.-Y. Yuen, Host and viral determinants for efficient SARS-CoV-2 infection of the human lung, Nat. Commun. 12 (2021) 134.

[27] H. Shuai, H. Chu, Y. Hou, D. Yang, Y. Wang, B. Hu, X. Huang, X. Zhang, Y. Chai, J.-P. Cai, J.F.-W. Chan, K.-Y. Yuen, Differential immune activation profile of SARS-CoV-2 and SARS-CoV infection in human lung and intestinal cells: implications for treatment with IFN-β and IFN inducer, J. Infect. 81 (2020) e1–e10.

[28] H. Chu, J. Fuk-Woo Chan, Y. Wang, T. Tsz-Tai Yuen, Y. Chai, H. Shuai, D. Yang, B. Hu, X. Huang, X. Zhang, Y. Hou, J.P. Cai, A.J. Zhang, J. Zhou, S. Yuan, K. Kai-Wang To, I. Fan-Ngai Hung, T.T. Cheung, A. Tsui-Lin Ng, I. Hau-Yee Chan, I. Yu-Hong Wong, S. Ying-Kit Law, D. Chi-Chung Foo, W.K. Leung, K.Y. Yuen, SARS-CoV-2 induces a more robust innate immune response and replicates less efficiently than SARS-CoV in the human intestines: An ex vivo study with implications on pathogenesis of COVID-19, Cell. Mol. Gastroenterol. Hepatol. 11 (2021) 771–781.

[29] J.F.-W. Chan, C.C.-Y. Yip, K.K.-W. To, T.H.-C. Tang, S.C.-Y. Wong, K.-H. Leung, A. Y.-F. Fung, A.C.-K. Ng, Z. Zou, H.-W. Tsoi, Improved molecular diagnosis of COVID-19 by the novel, highly sensitive and specific COVID-19-RdRp/Hel real-time reverse transcription-PCR assay validated in vitro and with clinical specimens, J. Clin. Microbiol. 58 (2020) e00310–e320.

[30] D. Wang, Q. Sun, M.J. Hokkanen, C. Zhang, F.-Y. Lin, Q. Liu, S.-P. Zhu, T. Zhou, Q. Chang, B. He, Q. Zhou, L. Chen, Z. Wang, R.H.A. Ras, X. Deng, Design of robust superhydrophobic surfaces, Nature 582 (2020) 55–59.

[31] P.A. Zhu, T.T. Kong, X. Tang, L.Q. Wang, Well-defined porous membranes for robust omniphobic surfaces via microfluidic emulsion templating, Nat. Commun. 8 (2017) 15823.

[32] C. Peng, Z. Chen, M.K. Tiwari, All-organic superhydrophobic coatings with mechanochemical robustness and liquid impalement resistance, Nat. Mater. 17 (2018) 355–360.

[33] J.C. Prata, A.L.P. Silva, T.R. Walker, A.C. Duarte, T. Rocha-Santos, COVID-19 pandemic repercussions on the use and management of plastics, Environ. Sci. Technol. 54 (2020) 7760–7765.